Coupling between mesoscopic dynamics and shear stress of room-temperature ionic liquid

Tsuyoshi Yamaguchi

Graduate School of Engineering, Nagoya University, Furo-cho B2-3 (611), Chikusa, Nagoya, Aichi 464-8603, Japan.

E-mail: yamaguchi.tsuyoshi@material.nagoya-u.ac.jp

Molecular dynamics (MD) simulation is performed on two imidazolium-based ionic liquids, one of which possesses a long alkyl chain whereas the other does not, and the coupling between the liquid structure and the shear stress is examined by means of cross-correlation analysis. The former liquid exhibits a prepeak representing the polar-nonpolar domain structure whereas the latter does not. The relaxation of the intermediate scattering function at the prepeak is slower than those of other microscopic structures. Nonetheless, the principal part of the viscoelastic relaxation is ascribed to the relaxation of the charge-alternation mode in both liquids. In particular, the dynamics of the domain structure hardly seems to affect the viscosity of the ionic liquid with a long alkyl chain, although the cross correlation between the shear stress and the domain mode exists and the relaxation of the cross correlation with the domain mode is far slower than that with the charge alternation mode. The absence of the domain dynamics in the viscoelastic relaxation is ascribed to the decoupling between the relaxations of the short- and the long-range structures.

Graphic Abstract

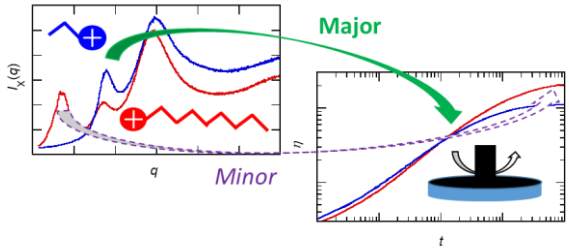

Highlights

Shear viscosity of ionic liquid is governed by dynamics of charge-alternation mode irrespective of the presence of domain structure

I. Introduction

It is well established nowadays that room-temperature ionic liquids (RTILs) with a long alkyl chain exhibit a characteristic mesoscopic structure composed of polar and nonpolar domains.[1,2,3,4] Ionic moieties of RTILs tend to gather through the electrostatic interaction, and the nonpolar alkyl groups expelled from the polar moieties also gets close to each other. Because of the covalent bond between the cationic and the alkyl groups, however, the scale of the separation between these groups is limited within the mesoscopic scale. In this sense, the mesoscopic structure of RTILs resembles those of surfactant solutions and diblock copolymers.[5]

The presence of the mesoscopic domain structure of RTIL is experimentally probed through the X-ray or neutron scattering experiment.[6,7] In addition to the strong peak at 10 – 20 nm^{-1} observed in various liquids, RTILs with a long alkyl chain exhibit a peak at several nm^{-1}, which is called "prepeak". With increasing the alkyl chain length, the prepeak shifts to lower-q, and its peak height grows, reflecting the development of the domain structure.

The dynamics of the domain structure can be determined by means of quasielastic scattering. Such experiments were actually performed by Kofu and coworkers, and they demonstrated that the relaxation of the domain structure is much slower than microscopic structural relaxations.[8,9]

Given that various properties, including static and dynamic ones, of the domain structure of RTILs are clarified, the next question is how the domain structure affects various macroscopic properties. In particular, the influence of the domain structure on shear viscosity is quite interesting, because the domain structure of RTILs resembles the mesoscopic structure of surfactant solution that gives rise to its large structural viscosity.[5]

A systematic experimental study on the relation between the domain structure and the shear viscosity was performed by Rocha and coworkers.[10] They measured the shear viscosity and the small-angle X-ray scattering (SAXS) of two series of imidazolium-based RTILs. The first series is that the lengths of the alkyl chains on the two nitrogen atoms of the imidazolium group are the same. The second one is that a

long alkyl chain is attached to one nitrogen atom, whereas the other nitrogen atom is methylated. Compared at the same total length of the alkyl chains, the latter exhibits the more developed domain structure, and the shear viscosity of the latter is higher than that of the former. It is thus suggested that the presence of the domain structure increases the shear viscosity of RTIL in some ways.

Shear viscosity is a transport property of liquid that reflects microscopic structural relaxation. It is defined as the linear response of the shear stress to weak shear flow. The linear response to the steady-state shear flow is equivalent to the time-integration of the linear response to instantaneous shear distortion. Microscopic liquid structure is distorted just after the application of the shear distortion, and the distorted structure yields non-zero shear stress. The distortion of the structure relaxes as time goes, and the shear stress decays to zero accordingly. In order to understand microscopic origin of shear viscosity, therefore, it is necessary to clarify what kind of microscopic structure is distorted to give shear stress.

The relaxation of the macroscopic shear stress can be determined experimentally with the measurement of frequency-dependent complex shear viscosity. The microscopic structural relaxation can be probed as a function of wavenumber by the quasielastic scattering spectroscopy. Comparing the relaxation functions obtained by these two experiments, therefore, we can estimate the contribution of the domain structure to shear viscosity.

We performed such a comparison on some RTILs through the combination of the quasielastic scattering experiment by Kofu and coworkers with transverse ultrasonic measurement in MHz region.[11,12] The results show that the viscoelastic relaxation is faster than that expected from the intermediate scattering function at the prepeak, suggesting rather limiting contribution of the domain dynamics to viscosity. On the other hand, Cosby and coworkers very recently performed the measurement of the viscoelastic relaxation of some RTILs at lower temperatures including supercooled conditions, and found bimodal relaxation when the alkyl chain of the cation is long.[13] They assigned the slower mode to the domain dynamics, although the direct comparison with the quasielastic scattering experiment was not performed.

We also calculated the dynamics of model ionic liquids using mode-coupling theory (MCT) for molecular liquids based on the interaction-site model.[14] The viscoelastic relaxation is bimodal when the nonpolar

group of the cation is sufficiently large, and the slower mode is assigned to the domain dynamics as was proposed by Cosby and coworkers. In addition, we found an indirect mechanism for the domain structure to increase the shear viscosity. Due to the geometrical restriction of the domain structure, the microscopic dynamics of the charge-alternation mode is retarded, which leads to the increase in viscosity.

We recently proposed a novel theoretical formalism that can extract the microscopic structure governing the shear viscosity using molecular dynamics (MD) simulation without invoking MCT approximation.[15] The formalism was then applied to Lennard-Jones (LJ) liquid,[16] water[17] and methanol,[15] and clarified the specific role of the hydrogen-bonding structure in the shear viscosity of the latter two hydrogen-bonding liquids.

In this work, we apply the same formalism to realistic model RTILs, and examine the direct coupling between shear stress and domain structure. MD simulation runs are performed on two RTILs. The first one is 1-ethyl-3-methylimidazolium bis(trifluoromethylsulfonyl)amide (emimTFSA), and the second one is 1-methyl-3-octylimidazolium TFSA (omimTFSA). As will be shown later, the latter exhibits the prepeak structure whereas the former does not. The role of the domain structure in viscosity will be analysed in detail based on the comparison between results on these two RTILs.

II. Theoretical Background

Kubo-Green formula describes the steady-state shear viscosity, η_0, in terms of the time correlation function of the shear stress tensor, $\mathbf{P}^{(s)}$, as[18,19]

$$\eta_0 = \int_0^\infty dt\, G(t), \tag{1}$$

$$G(t) \equiv \frac{V}{k_B T} \langle P_{xy}^{(s)} e^{iLt} P_{xy}^{(s)} \rangle, \tag{2}$$

where V, k_B, T, and L stand for the volume of the system, the Boltzmann constant, the absolute temperature, and the Liouvillian operator, respectively. The shear stress tensor is defined as the symmetric and traceless part of the pressure tensor. Equation (2) is based on the linear response theory that relates the linear

response to weak shear flow with the fluctuation of the shear stress without the flow. To understand the shear viscosity from the microscopic view is thus equivalent to relating the dynamics of the shear stress to that of microscopic liquid structure.

We employ here two-body density as the descriptor of the liquid structure. The two-body density can be described in both real and reciprocal spaces. The real-space definition is given by

$$\rho_{\alpha\gamma}^{(2r)}(\mathbf{r}) \equiv \frac{1}{V}\int d\mathbf{R}\, \rho_\alpha(\mathbf{R}+\mathbf{r})\, \rho_\gamma(\mathbf{R}), \tag{3}$$

where α and γ indicate an interaction-site or a group of interaction-sites, and $\rho_\alpha(\mathbf{r})$ stands for the density field of α. The reciprocal-space description is

$$\rho_{\alpha\gamma}^{(2)}(\mathbf{q}) \equiv \tilde{\rho}_\alpha^*(\mathbf{q})\tilde{\rho}_\gamma(\mathbf{q}), \tag{4}$$

where $\tilde{\rho}(\mathbf{q})$ means the density field in the reciprocal space, and the asterisk denotes the complex conjugate. The absolute value of the vector $\mathbf{q}$, denoted as q, equals to $2\pi/\lambda\sin(\theta/2)$ in scattering experiments, where λ and θ indicate the wavelength of the incident beam and the scattering angle, respectively. The two representations, eqs. (3) and (4), are related with each other through the Fourier transformation. It is to be noted here that the vector space spanned by the fluctuation of the two-body density does not depend on the representations of the real or the reciprocal spaces.

The equilibrium average of the two-body density defines the pair correlation functions. In the real space, the partial radial distribution function, $g_{\alpha\gamma}(r)$, is given by

$$\langle\rho_{\alpha\gamma}^{(2r)}(\mathbf{r})\rangle \equiv \bar{\rho}_\alpha\delta_{\alpha\gamma}\delta(\mathbf{r}) + \bar{\rho}_\alpha\bar{\rho}_\gamma g_{\alpha\gamma}(r), \tag{5}$$

where $\bar{\rho}_\alpha$ stands for the number density of α. The absolute value of the vector $\mathbf{r}$ is denoted as r here. In the reciprocal space, the two-body density is related to the partial static structure factor, $\chi_{\alpha\gamma}(q)$, as

$$\chi_{\alpha\gamma}(q) = \frac{1}{V}\langle\rho_{\alpha\gamma}^{(2)}(\mathbf{q})\rangle. \tag{6}$$

It is to be noted here that the normalization factor, $1/V$ in eq. (6), varies among literatures.

The projection operator onto the space spanned by the fluctuation of the two-body density, denoted as $P^{(2)}$, is inserted into the rhs. of eq. (2) as

$$G(t) \cong \frac{V}{k_BT}\langle P_{xy}^{(s)} P^{(2)} e^{iLt} P_{xy}^{(s)}\rangle, \tag{7}$$

where detailed descriptions of the projection-operator formalism are given in literatures.[18] After some calculations, the shear relaxation function, $G(t)$, is approximated in the reciprocal-space representation as[15]

$$G(t) \cong \sum_{\alpha\gamma} \int d\mathbf{q} \frac{q_x q_y}{q^2} V_{\alpha\gamma}(\mathbf{q}) \rho^{(2)}_{\eta,\alpha\gamma}(q,t), \tag{8}$$

$$\rho^{(2)}_{\eta,\alpha\gamma}(q,t) \equiv \frac{V}{k_B T} \frac{q^2}{q_x q_y} \langle \delta\rho^{(2)}_{\alpha\gamma}(\mathbf{q}) e^{iLt} P^{(s)}_{xy} \rangle, \tag{9}$$

$$\delta\rho^{(2)}_{\alpha\gamma}(\mathbf{q},t) \equiv \rho^{(2)}_{\alpha\gamma}(\mathbf{q},t) - V\chi_{\alpha\gamma}(q). \tag{10}$$

The function $\rho^{(2)}_{\eta,\alpha\gamma}(q,t)$ describes the transient response of the structure factor along the compression axis after the instantaneous shear distortion, and the function $V_{\alpha\gamma}(\mathbf{q})$ denotes the contribution of the distorted structure to the shear stress. The explicit expression of the latter in terms of the correlation functions is omitted here for brevity.

The real-space version of the response of the pair correlation, $g_{\eta,\alpha\gamma}(r,t)$, is defined as[17]

$$g_{\eta,\alpha\gamma}(r,t) \equiv \frac{|\mathbf{r}|^2}{\bar{\rho}_\alpha \bar{\rho}_\gamma k_B T r_x r_y} \langle \delta\rho^{(2r)}_{\alpha\gamma}(\mathbf{r}) e^{iLt} P^{(s)}_{xy} \rangle, \tag{11}$$

which describes the anisotropic distortion of the radial distribution function under weak shear flow. Both $\rho^{(2)}_{\eta,\alpha\gamma}(q,t)$ and $g_{\eta,\alpha\gamma}(r,t)$ can be evaluated directly by means of MD simulation.

Introducing the approximations employed in MCT, the cross-correlation function in the reciprocal space is approximated in terms of the partial intermediate scattering functions, $F_{\alpha\gamma}(q,t)$, as[15]

$$\rho^{(2)}_{\eta,\alpha\gamma}(q,t) = -q \sum_{\mu\nu} F_{\alpha\mu}(q,t) \frac{dc_{\mu\nu}(q)}{dq} F_{\nu\gamma}(q,t), \tag{12}$$

$$F_{\alpha\gamma}(q,t) \equiv \frac{1}{V} \langle \tilde{\rho}^*_\alpha(\mathbf{q}) e^{iLt} \tilde{\rho}_\gamma(\mathbf{q}) \rangle. \tag{13}$$

Here, the direct correlation function, $c_{\alpha\gamma}(q)$, is defined as[20]

$$\mathbf{c}(q) \equiv [\boldsymbol{\rho}^{-1} - \boldsymbol{\chi}^{-1}(q)], \tag{14}$$

where $\mathbf{c}(q)$ and $\boldsymbol{\chi}(q)$ are square matrices labelled by interaction sites, and $\boldsymbol{\rho}$ is the diagonal matrix whose diagonal component is equal to $\bar{\rho}_\alpha$. Equation (12) states that the response of the two-body density to the instantaneous shear deformation is described by the square of the intermediate scattering function.

The expression of $G(t)$, eq. (8), is further approximated accordingly as[21]

$$G(t) \cong \frac{k_B T}{60\pi^2} \int_0^\infty dq\, q^4 \mathrm{Tr}\left[\frac{d\mathbf{c}(q)}{dq} \cdot \mathbf{F}(q,t)\right]^2. \quad (15)$$

The comparison of $G(t)$ with $F(q,t)$ at various q-values based on eq. (15) thus gives information on the length scale of the microscopic structure that is important in determining the shear viscosity.

III. Simulation Methods

The molecular models of the ionic liquids, emimTFSA and omimTFSA, are the united atom models proposed by Zhong and coworkers.[22] In these models, CH_2 and CH_3 groups of the imidazolium cations and CF_3 groups of the TFSA anion are treated as the united atoms, and the magnitude of the total charge on an ion is reduced to 0.8*e*, where *e* stands for the charge of a proton. It has been demonstrated that these models can reproduce the temperature dependence of the shear viscosity fairly well.

The systems we treat are composed of 1000 ion pairs, which were filled into a cubic cell with the periodic boundary condition. The MD simulation runs were performed under NPT ensemble, where the temperature and the pressure of the systems were 353 K and 1 bar, respectively. We performed the simulation at the elevated temperature because the faster structural relaxation under the higher temperature improves the statistical qualities of the correlation functions at a given total length of the run. A production run of 1 μs length was performed for each liquid after an equilibration run of 100 ns length.

All the simulation runs were performed using GROMACS 5.1.2 package.[23] The equation of motion was integrated using the leap-frog algorithm with the time step of 1 fs. The pressure tensor was calculated at every second step and the summation over 50 consecutive steps, together with the instantaneous value, was recorded at every 100th step. The coordinates of all the atoms were stored at every 10000 step. The temperature and the pressure of the system were controlled by Nosé-Hoover thermostat and Parrinello-Rahman barostat, respectively. The long-range Coulombic interaction was evaluated by the Particle-Mesh-Ewald method with the mesh spacing of 0.12 nm. The short-range part of the intermolecular interaction was cut off at 1.2 nm. The bond lengths associated with hydrogen atoms were fixed using

LINCS algorithm,[24] and the other intramolecular degrees of freedom were treated as flexible.

In the analyses of the density modes in the reciprocal space, the atoms are grouped together for simplicity. The number of groups are two in the case of emimTFSA, that is, the cation (C) and the anion (A) groups, whereas the atoms in omimTFSA are grouped into three, namely, the cationic (C), the nonpolar (N), and the anion (A) groups. The cationic and the nonpolar groups refer to the methylimidazolium and the octyl ones, respectively. The density mode of the group G is defined as

$$\tilde{\rho}_G(\mathbf{q}) \equiv \sum_{j\in G} b_j \exp\left[i\mathbf{q}\cdot\mathbf{r}_j\right], \tag{16}$$

where $\mathbf{r}_j$ stands for the position of the atom j belonging to the group G. As the weighting parameter b_j, we employed the X-ray scattering length, which is proportional to the number of electrons on the atom. The numbers of electrons were then calculated from the partial charges used for the intermolecular interaction by subtracting the partial charge on a united atom from the sum of the charges of nuclei belonging to the united atom. In the real-space analysis, the positions of the C and A groups are represented by the geometric center of the five atoms of the imidazolium ring and the central nitrogen atom of the TFSA ion, respectively.

IV. Results and Discussion

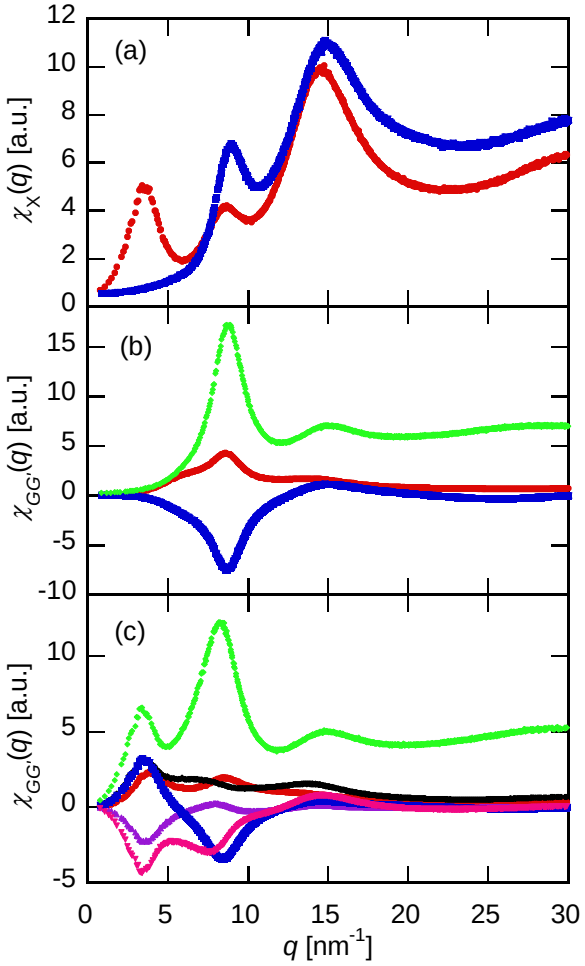

Figure 1. The static structure factors are plotted. The X-ray total structure factors of emimTFSA (blue) and omimTFSA (red) are shown in panel (a). The X-ray structure factor of emimTFSA is separated into C-C (red), C-A (blue) and A-A (green) components in panel (b), and that of omimTFSA is separated into C-C (red), C-A (blue), A-A (green), N-N (black), C-N (purple), and A-N (pink) ones in panel (c).

The X-ray structure factors of two RTILs calculated by our MD simulations are shown in Fig. 1a. Three peaks are found in the structure factor of omimTFSA, whereas the lowest-q one is missing in that of emimTFSA. The structure factor of RTILs has been studied intensively, and the origins of these peaks are now well established.[4,14] The lowest-q peak at 3 nm^{-1}, which exists only in omimTFSA, is called "prepeak", and it reflects the mesoscopic structure composed of polar and nonpolar domains. The second peak at q = 8 nm^{-1} is called "charge-alternation peak", and it originates from the charge-density mode. The third peak at q = 14 nm^{-1} is called "adjacent peak", and it is assigned to the number density of atoms.

The assignments described above are supported by the partial structure factors shown in Figs. 1b and 1c. All the components are positive at the adjacent peak, which means that the peak originates from the number density of atoms irrespective of their characters. The C-A component is negative at the charge-alternation peak, indicating that the peak reflects the contrast between the C and A groups. At the prepeak of omimTFSA, C-N and A-N components are negative while the C-A correlation is positive. The prepeak is thus assigned to the contrast between the polar (C+A) and nonpolar (N) domains.

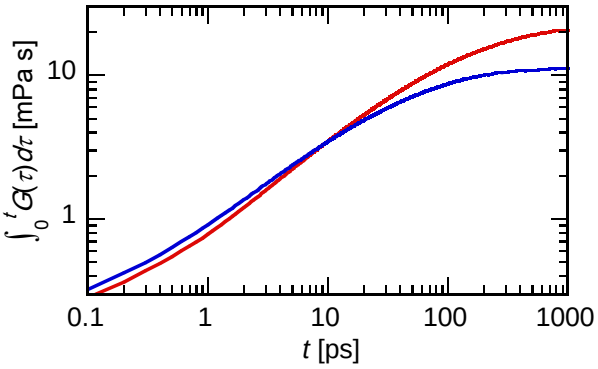

Figure 2. The running integrals of $G(t)$ of emimTFSA (blue) and omimTFSA (red) are plotted as the functions of time.

The running integrals of the shear relaxation function, $G(t)$, of the two RTILs are shown in Fig. 2. The correlation functions $G(t)$ were evaluated according to the definition of eq. (2). Their long-time limiting values are equal to the steady-state shear viscosity, η_0. The values of η_0 of emimTFSA and omimTFSA determined in this work are 10.9 mPa s and 20.3 mPa s, respectively, which are a little larger than the corresponding values reported by Zhong and coworkers using the same models, 8.3 mPa s and 18.5 mPa s, respectively.[22] Considering the statistical difficulty in determining the time correlation function of collective quantities in slow-relaxing systems, we consider that the agreement between the values of Zhong and coworkers and those of ours is acceptable. The densities of emimTFSA and omimTFSA obtained in this work are 1479±4 kg/m^3 and 1274±3 kg/m^3, respectively, which are in good agreement with those of Zhong and coworkers, 1477 kg/m^3 and 1278 kg/m^3, respectively.[22] The numbers after '±' indicates the standard deviation here.

It is well-known that the viscosity of imidazolium-based RTILs increases with increasing the length of the alkyl chain,[25] and our simulation reproduces the experimental trend. Looking at the short-time part of the running integral at $t < 10$ ps, however, it should be noticed that the short-time viscosity of emimTFSA is larger than that of omimTFSA. It means that the plateau modulus of the former is larger than that of the latter, which in turn is ascribed to the stronger intermolecular Coulombic interaction of the former due to the higher ionic density. The effect of the larger relaxation time of omimTFSA overwhelms the weaker mean intermolecular interaction to make the shear viscosity larger. Although the larger viscosity of RTILs with a longer alkyl chain was ascribed to the van der Waals interaction between alkyl chains in early days of studies on RTIL, the mean intermolecular interaction represented as the plateau modulus decreases actually with lengthening the alkyl chain. We experimentally measured the shear relaxation spectra of a series of imidazolium-based RTILs with changing the lengths of the alkyl chain, and found that the increase in the shear relaxation time with lengthening the alkyl chain is stronger than that of the shear viscosity.[26,27] Our simulation result on $G(t)$ shown in Fig. 2 is thus in harmony with the shear relaxation experiment.

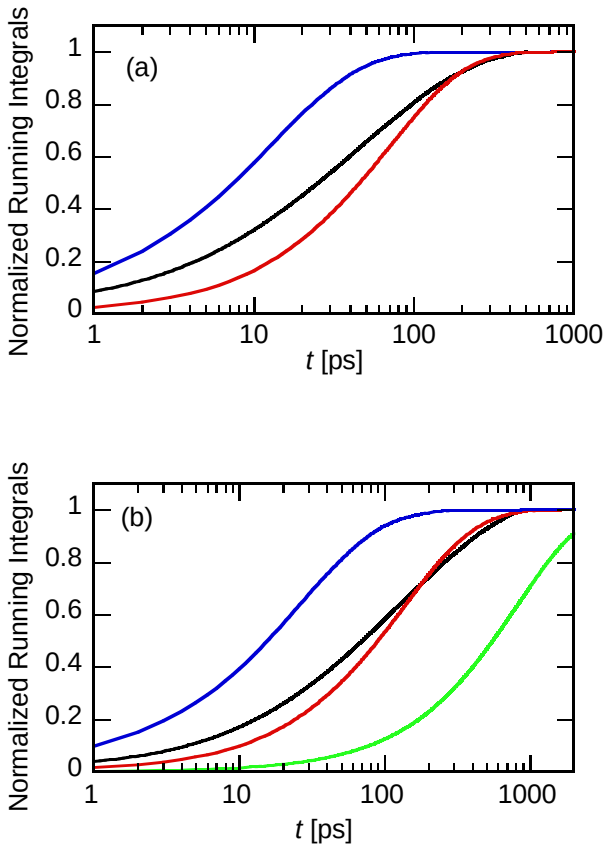

Figure 3. The normalized running integral of $G(t)$ (black) is plotted together with those of the square

of X-ray intermediate scattering functions at three peaks, namely, the adjacent peak (blue), the charge-alternation one (red), and the prepeak (green). The results on emimTFSA and omimTFSA are shown in panels (a) and (b), respectively.

Figure 3 compares the shear relaxation with the structural relaxation represented as the intermediate scattering function. We employ here the X-ray intermediate scattering function defined as

$$F_X(q,t) \equiv \frac{1}{V}\langle \tilde{\rho}_X^*(\mathbf{q}) e^{iLt} \tilde{\rho}_X(\mathbf{q})\rangle, \tag{17}$$

$$\tilde{\rho}_X(\mathbf{q}) \equiv \sum_{\text{all atoms}} b_j \exp\left[i\mathbf{q}\cdot\mathbf{r}_j\right], \tag{18}$$

for comparison. The running integrals of the squares of $F_X(q,t)$ are calculated at the two or the three peaks of the static structure factors, Fig. 1a, and plotted together with that of $G(t)$. The intermediate scattering function is squared based on the MCT idea, eq. (15).

As is shown in Fig. 3, the relaxation of $F_X(q,t)$ at the peaks becomes slower with decreasing q. The relaxation of omimTFSA at the prepeak is slower than that at the charge-alternation peak, which is consistent with the neutron spin echo (NSE) measurement reported by Kofu and coworkers.[9] Compared with $G(t)$, the relaxation of the shear stress occurs in the time scale similar to that of the charge-alternation mode. In particular, even though the domain structure relaxes much slower than the charge-alternation mode in omimTFSA, the relaxation of the shear stress does not follow the domain dynamics.

We have experimentally compared the shear relaxation with the intermediate scattering function at the prepeak for some RTILs with a long alkyl chain.[11,12] The shear relaxation is much faster than that predicted from the intermediate scattering function at the prepeak, and it is rather close to that at the charge-alternation mode. The correspondence between the shear relaxation and the dynamics at the charge-alternation mode demonstrated in Fig. 3 is thus consistent with our experiments.

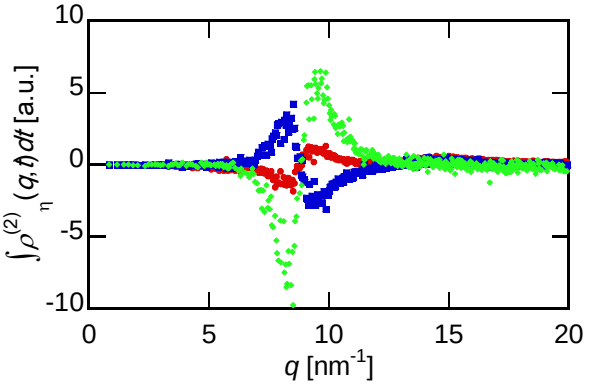

Figure 4. The cross-correlation functions $\rho_\eta^{(2)}(q,t)$ of emimTFSA integrated over time from t = 0 to 500 ps are shown. The C-C, C-A, and A-A components are plotted with red, blue, and green symbols, respectively.

The cross-correlation functions $\rho_\eta^{(2)}(q,t)$ of emimTFSA are plotted in Fig. 4. The functions are integrated over time up to 500 ps, at which the relaxation of $G(t)$ is almost completed as is exhibited in Fig. 2. The profiles in Fig. 4 are thus regarded as the distortion of the structure factor under steady-state shear flow along the compression axis.

The profiles in Fig. 4 appear quite simple. At first, the response is almost limited within the charge-alternation mode of the static structure factor. It is consistent with the picture obtained from the time profiles in Fig. 3a that the relaxation of the shear stress is as slow as that of the charge-alternation mode. Second, the shape of the profiles in Fig. 4 resembles the negative of the derivative of the charge-alternation peak in Fig. 1b. These profiles indicate that the charge-alternation peak shifts to higher-q along the compression axis, whereas it shifts to lower-q along the expansion axis.

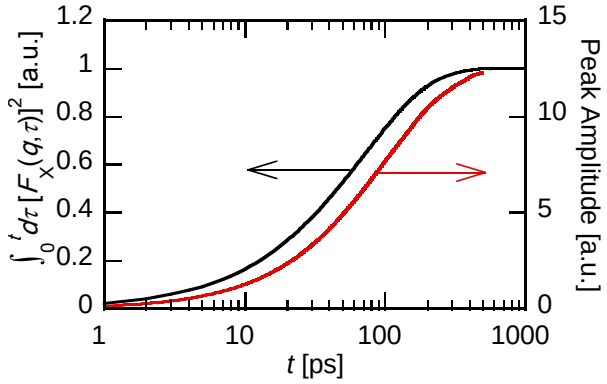

Figure 5. The running integral of the amplitude of $\rho^{(2)}_{\eta,AA}(q,t)$ of emimTFSA at the charge alternation mode (red) is compared with that of $[F_X(q,t)]^2$ (black).

The time profile of the cross-correlation function is compared with the squared intermediate scattering function in Fig. 5. Here, the amplitude of $\rho^{(2)}_{\eta,AA}(q,t)$ at the charge alternation mode is defined as the difference between the averages around the positive peak at 9.2 – 9.8 nm^{-1} and the negative peak at 8.0 – 8.6 nm^{-1}. Although the relaxation of the cross correlation is a little slower, it approximately follows the relaxation of the squared intermediate scattering function at the corresponding peak as is suggested by eq. (12).

The picture of shear viscosity of emimTFSA revealed by the cross-correlation analysis is rather simple. The liquid structure is uniformly compressed along the compression axis just after the instantaneous shear deformation. The peaks of the structure factor shift to higher-q accordingly. The shifted peaks relax with their respective time constant determined by the corresponding intermediate scattering function. Since the charge-alternation mode is the slowest microscopic mode of the system, the relaxation of its peak shift dominates the slowest mode of the viscoelastic relaxation. The mechanism of shear viscosity of emimTFSA is thus similar to that of LJ liquid where the slowest viscoelastic relaxation mode is coupled to the shift of the main peak of the static structure factor.[16]

The idea presented above on emimTFSA that the charge-alternation mode governs the viscoelastic relaxation because it is the slowest microscopic relaxation cannot hold on omimTFSA in principle. The relaxation of the intermediate scattering function at the prepeak is slower than that at the charge-alternation mode as is exhibited in Fig. 3b. If the slowest microscopic relaxation governs the slowest mode of the viscoelastic relaxation, therefore, it must be the domain dynamics that determines the shear viscosity of omimTFSA. However, the shear relaxation of omimTFSA actually follows the dynamics of the charge-alternation mode, regardless of the presence of the slower domain dynamics. Hereafter we shall resolve the rather puzzling result on omimTFSA based on the cross-correlation analysis.

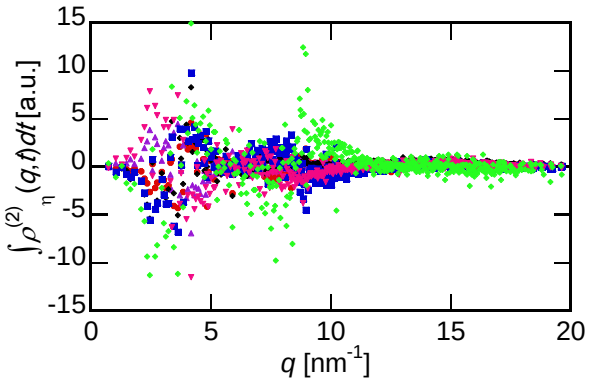

Figure 6. The cross-correlation functions $\rho_{\eta}^{(2)}(q,t)$ of omimTFSA integrated over time from t = 0 to 2 ns are shown. The colors of the symbols are used in the same way as those of Fig. 1c, that is, C-C (red), C-A (blue), A-A (green), N-N (black), C-N (purple), and A-N (pink).

The cross-correlation function $\rho_{\eta}^{(2)}(q,t)$ of omimTFSA is integrated over time between t = 0 and 2 ns, and it is plotted in Fig. 6. The upper limit of the time-integral, t = 2 ns, is chosen so that the relaxation of $\rho_{\eta}^{(2)}(q,t)$ is completed and the profile describes the structural distortion under steady-state shear flow.

Although the statistical quality of the profile is not so good, the responses are observed clearly at both the prepeak and the charge-alternation peak. The profiles at both peaks are derivative-shaped, indicating the high-q shift of both peaks along the compression axis. In particular, the response of the domain structure to shear flow is present.

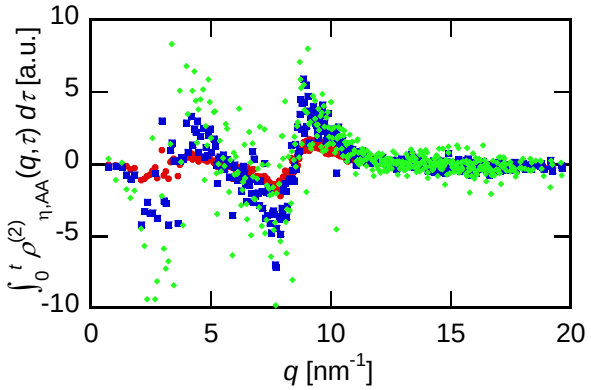

Figure 7. The A-A component of the cross-correlation functions $\rho_{\eta,AA}^{(2)}(q,t)$ of omimTFSA integrated over time from t = 0 are shown. The values of the upper limit of the time-integral are 100 ps (red), 500 ps (blue) or 2 ns (green).

Figure 7 shows the A-A component of the time-integrated cross-correlation function at three different values of the upper limit of the time integral. The derivative-shaped profiles at both peaks grow with time. The blue (500 ps) and the green (2 ns) profiles are almost the same at the charge-alternation peak, which indicates that the relaxation of the profile at the charge-alternation mode is almost completed within 500 ps. On the other hand, the profile at the prepeak develops from 500 ps to 2 ns. The relaxation of the response of the domain structure to shear distortion is slower than that of the charge-alternation mode.

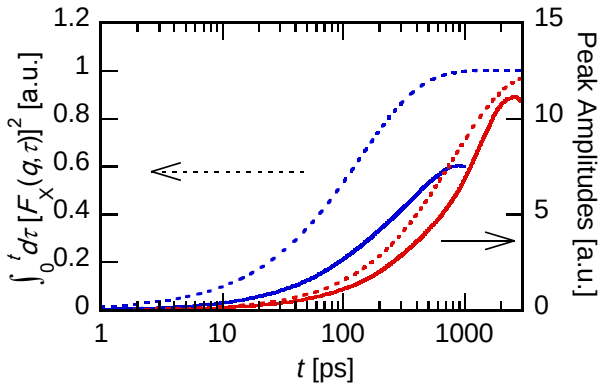

Figure 8. The running integrals of the amplitude of $\rho^{(2)}_{\eta,AA}(q,t)$ of omimTFSA (solid) are compared with those of $[F_X(q,t)]^2$ (dotted). The functions at the prepeak and the charge-alternation peak are drawn with red and blue colors, respectively.

The running integrals of the amplitudes of the derivative-shaped profiles of $\rho^{(2)}_{\eta,AA}(q,t)$ at two peaks are calculated, and they are compared with the running integrals of $[F_X(q,t)]^2$ at the corresponding peaks in Fig. 8. The amplitude at the prepeak is the difference between the averaged values at 3.5 – 4.5 nm^{-1} and 2.0 – 3.0 nm^{-1}, and that at the charge-alternation peak is those at 8.8 – 9.8 nm^{-1} and 7.2 – 8.2 nm^{-1}. As is the case of emimTFSA, the relaxation of $\rho^{(2)}_{\eta,AA}(q,t)$ follows that of the intermediate scattering function at the corresponding peak, although the former is a little slower.

The cross correlation between the shear stress and the domain structure exists in omimTFSA, and its relaxation is as slow as that predicted from the intermediate scattering function at the prepeak. Nonetheless, the slow relaxation of the domain structure is not reflected in the shear relaxation function, $G(t)$. In eq. (8), $\rho^{(2)}_{\eta,\alpha\gamma}(q,t)$ in the integral shows slow relaxation at the prepeak, but the corresponding

slow relaxation is absent in $G(t)$ at lhs. It suggests that the coupling strength $V_{\alpha\gamma}(\mathbf{q})$ is small at the prepeak. Physically speaking, the domain structure of omimTFSA is so soft that its distortion hardly yields shear stress.

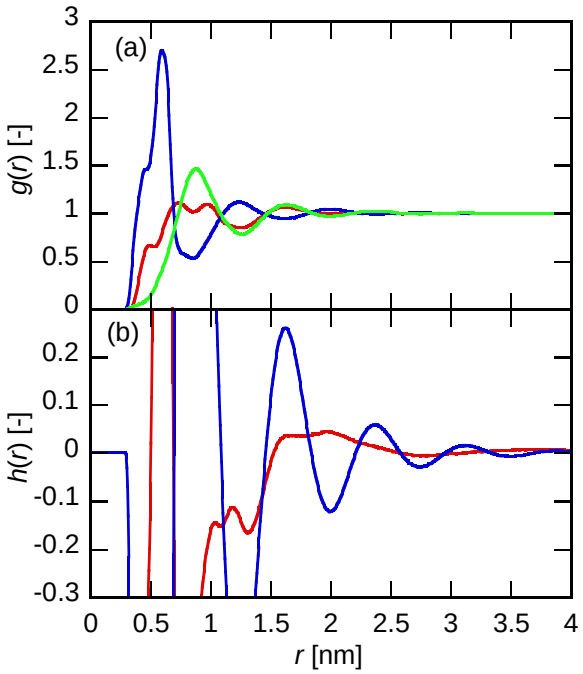

Figure 9. The C-C (red), C-A (blue), and A-A (green) components of the radial distribution functions are plotted in panel (a), whereas the charge-alternation [$h_{CC}(r)$ - $2h_{CA}(r)$ + $h_{AA}(r)$, blue] and the domain [$h_{CC}(r)$ + $2h_{CA}(r)$ + $h_{AA}(r)$, red] components of the total correlation functions are shown in panel (b).

The coupling between the shear stress and domain dynamics is analysed hereafter also in the real-space representation. Figure 9a shows the radial distribution functions between ionic groups. A strong contact peak is observed at 0.6 nm in $g_{CA}(r)$. The alternating oscillation structure of the diagonal (CC and AA) and the off-diagonal (CA) components is also noticed.

The linear combinations of the total correlation functions, $h_{\alpha\gamma}(r) \equiv g_{\alpha\gamma}(r) - 1$, are calculated from the radial distribution functions, and they are shown in Fig. 9b. The component $h_{AA}(r)$ - $2h_{CA}(r)$ + $h_{AA}(r)$ stands for the charge-density mode. It shows an oscillation with the wavelength of ~ 0.8 nm, which corresponds to the charge-alternation peak of the static structure factor. The component $h_{AA}(r)$ + $2h_{CA}(r)$ + $h_{AA}(r)$ is related to the domain structure, because it represents the autocorrelation of the density of the charged groups. The domain component exhibits the oscillation with a different wavelength, ~ 2 nm,

which corresponds to the prepeak of the static structure factor.

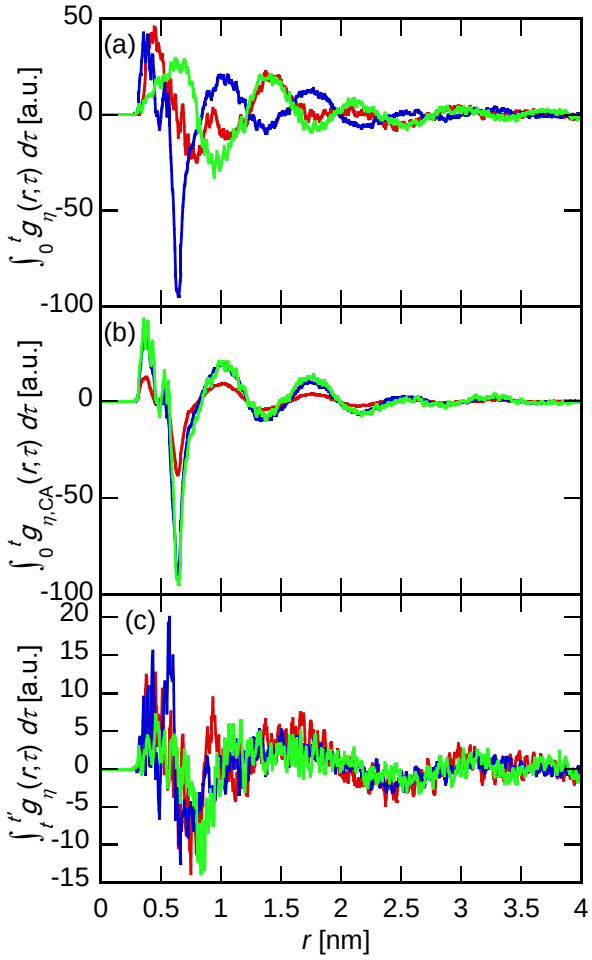

Figure 10. The cross-correlation functions in the real-space representation, $g_\eta(r,t)$, are integrated over time and plotted as the functions of r. The integrals over t = 0 to 2 ns are shown in panel (a), where the red, blue, and green curves indicate the C-C, C-A, and A-A components, respectively. The C-A components with the different values of the upper limit of the time-integral, 100 ps (red), 500 ps (blue), and 2 ns (green) are shown in panel (b). The time-integrals from 500 ps to 2 ns are shown in panel (c), where the meanings of the colors are the same as those in panel (a).

The real-space version of the cross-correlation function, $g_\eta(r,t)$, is exhibited in Fig. 10. The time-integral from t = 0 to 2 ns is shown in Fig. 10a, which corresponds to the response of the pair correlation function along the compression axis under steady-state shear flow. The profiles resemble the derivative of the radial distribution function shown in Fig. 9a, which means that the deformation of the pair correlation under shear flow is approximately regarded as the uniform compression.

The time-development of the cross-correlation function is analyzed in Fig. 10b by comparing the time-integrated functions with different values of the upper limit of the integral. Based on the agreement of the functions at 500 ps and 2 ns, it is recognized that the integral is almost converged within 500 ps. In particular, the strong response within the first solvation shell is completed within 500 ps. The convergence of the time-integral is also observed in the case of the cross-correlation function in the reciprocal space at the charge-alternation mode, and the dynamics of $g_{\eta,CA}(r,t)$ appears to follow that of $\rho_{\eta}^{(2)}(q,t)$ at the charge-alternation mode.

Closely looking at Fig. 10b, however, a small difference is found at larger *r* between the functions at 500 ps and 2 ns. In order to extract the slow relaxation dynamics, the time integral from t = 500 ps to 2 ns is calculated and plotted in Fig. 10c. The profiles of long wavelength are clearly observed. The wavelength is close to that of the domain mode of the total correlation function shown in Fig. 9b. The amplitudes and the phases of the three components, C-C, C-A, and A-A, are almost the same at large distance, indicating that the large-scale slow dynamics of $g_{\eta}(r,t)$ does not accompany the change in the charge density. Therefore, the slow dynamics extracted in Fig. 10c corresponds to the slow relaxation of $\rho_{\eta}^{(2)}(q,t)$ at the prepeak.

An important point in Fig. 10c is that the amplitude of the slow mode within the first solvation shell is small. Since strong intermolecular momentum transfer usually occurs between a pair of molecules contacted with each other, the small amplitude at the first solvation shell explains the weak coupling of the slow domain mode with the shear stress. Although the long-range Coulombic interaction also works in RTILs, its coupling with the domain mode is not expected, either, because the slow domain dynamics hardly accompanies the change in the charge density. Physically speaking, the short-range structure within the polar domain relaxes before the relaxation of the domain structure is completed, so that the shear stress is hardly coupled to the domain dynamics.

MD simulation in this work showed that the slow domain dynamics of omimTFSA is little coupled to the viscoelastic relaxation, and it is consistent with our previous experimental works based on the comparison between the shear relaxation spectrum in the MHz region and the intermediate scattering

function determined by NSE spectroscopy.[11,12] On the other hand, Cosby and coworkers measured the viscoelastic spectra of some RTILs at lower temperatures using a mechanical rheometer. They found an additional slow mode when the alkyl chain attached to the imidazolium cation is long, and they assigned the slow mode to the domain dynamics.[13] We consider that an important difference between their works and ours is that in the temperature. Both our experiment and MD simulation are performed near the room temperature at which the relaxation time of the system is in the ns scale. On the other hand, the rheological experiment by Cosby and coworders was performed in low-temperature region including supercooled one where the relaxation time is in the ms scale. Even though the coupling between the shear stress and the domain dynamics is weak around the room temperature, the coupling may be strengthened at the lower temperatures. Temperature effect is thus a remaining issue of our future work. On theoretical side, since direct MD simulation in the ms scale is difficult with current capacity of computers, combination with some analytical theories would be desirable to handle such slow dynamics. On experimental side, rheological measurements in the wide temperature region using spectrometer of wide frequency range will be required in order to examine the effect of the temperature.

Another important point to be noted is the relation with the stress-structure coupling in higher alcohols. The X-ray static structure factor of higher alcohols is characterized by the low-q prepeak.[28,29] Since the prepeak of higher alcohols originates in the mesostructure composed of the polar OH and the nonpolar alkyl groups, it has the similar character to that of RTILs with a long alkyl chain. The viscoelastic spectrum of higher alcohols exhibits a bimodal relaxation.[30,31,32] We have studied the origin of the two relaxation modes both experimentally[33] and theoretically,[34] and found that the slower mode of the viscoelastic relaxation is assigned to the structural dynamics at the prepeak. Although RTIL with a long alkyl chain and higher alcohols possess the prepeak structure in common, the dynamics at the prepeak plays different roles in the viscoelastic relaxation of these two classes of liquids. We are now undertaking the cross-correlation analysis of the stress-structure coupling of higher alcohols in order to clarify the microscopic origin of the difference.

V. Summary

MD simulation was performed on two RTILs, emimTFSA and omimTFSA, and the microscopic origin of the shear viscosity was examined through the analyses of the cross-correlation functions between the shear stress and the two-body density.

The X-ray structure factor of omimTFSA shows a low-q prepeak representing the mesoscopic structure composed of polar and nonpolar domains, whereas the prepeak is missing in emimTFSA. The intermediate scattering function at the prepeak relaxes much slower than other high-q peaks in the case of omimTFSA. Nevertheless, the viscoelastic relaxation of these two RTILs followed the intermediate scattering functions at the charge-alternation peak, irrespective of the presence of the slow domain dynamics.

The cross correlation between the charge-alternation mode and the shear stress gives a simple picture of the shear viscosity of RTILs. The charge-alternation peak shifts to higher-q along the compression axis just after the instantaneous shear deformation, and the anisotropic peak shift becomes the origin of the shear stress. The shifted peak then relaxes to the equilibrium position at the rate predicted by the intermediate scattering function.

The cross correlation between the domain structure and the shear stress is found in omimTFSA, and its relaxation is as slow as that expected from the intermediate scattering function at the prepeak. However, the viscoelastic relaxation of omimTFSA is completed before the relaxation of the domain structure, and the distortion of the domain structure hardly contributes to the shear stress. The analysis of the cross correlation in the real space resolves the puzzling result. The slow relaxation of the domain mode little accompanies the structural reorganization within the first solvation shell, which explains the weak contribution of the domain mode to the viscoelastic relaxation. The domain structure of omimTFSA is very soft, which is ascribed to the decoupling between the short- and long-range dynamics.

The MD simulation runs in this work are limited to the temperature higher than the ambient one due to

the limitation of computational resources. On the other hand, Cosby and coworkers reported the presence of a slow viscoelastic mode in the low-temperature region.[13] Therefore, the relation between the mesoscopic dynamics and the shear viscosity may be dependent on temperature, and the study of the temperature effects is a remaining issue of future works.

Conflicts of Interest

There are no conflicts of interest to declare.

Acknowledgments

TY is grateful to Prof. R. Böhmer (Tech. Univ. Dortmund) for sending the manuscript of Ref. 28 prior to publication. This work was supported by the Japan Society for the Promotion of Science (JSPS), KAKENHI Grant No. 16K05514.

References

[1] S. M. Urahata and M. C. C. Ribeiro, *J. Chem. Phys.*, 2004, **120**, 1855–1863.

[2] J. N. A. Canongia Lopes and A. A. H. Pádua, *J. Phys. Chem. B*, 2006, **110**, 3330–3335.

[3] R. Hayes, G. G. Warr and R. Atkin, *Chem. Rev.*, 2015, **115**, 6357–6426.

[4] H. K. Kashyap, J. J. Hettige, H. V. R. Annapureddy and C. J. Margulis, *Chem. Commun.*, 2012, **48**, 5103-5105.

[5] T. Witten and P. Pincus, *Structured Fluids: Polymers, Colloids, Surfactants*, Oxford University Press, 2004.

[6] A. Triolo, O. Russina, H. J. Bleif and E. DiCola, *J. Phys. Chem. B*, 2007, **111**, 4641−4644.

[7] O. Russina and A. Triolo, *Faraday Discuss.*, 2012, **154**, 97−109.

[8] O. Yamamuro, T. Yamada, M. Kofu, M. Nakakoshi and M. Nagao, *J. Chem. Phys.* 2011, **135**, 054508

[9] M. Kofu, M. Nagao, T. Ueki, Y. Kitazawa, Y. Nakamura, S. Sawamura, M. Watanabe and O. Yamamuro, *J. Phys. Chem. B*, 2013, **117**, 2773–2781.

[10] M. A. A. Rocha, C. M. S. S. Neves, M. G. Freire, O. Russina, A. Triolo, J. A. P. Coutinho and L. M. N. B. F. Santos, J. Phys. Chem. B, 2013, 117, 10889-10897.

[11] T. Yamaguchi, K. Mikawa, S. Koda, K. Fujii, H. Endo, M. Shibayama, H. Hamano and Y. Umebayashi, *J. Chem. Phys.*, 2012, **137**, 104511.

[12] T. Yamaguchi, T. Yonezawa and S. Koda, *Phys. Chem. Chem. Phys.*, 2015, **17**, 19126–19133.

[13] T. Cosby, Z. Vicars, Y. Wang and J. Sangoro, *J. Phys. Chem. Lett.*, 2017, **8**, 3544–3548.

[14] T. Yamaguchi, *J. Chem. Phys.*, 2016, **144**, 124514.

[15] T. Yamaguchi and A. Faraone, *J. Chem. Phys.*, 2017, **146**, 244506.

[16] T. Yamaguchi, *J. Chem. Phys.*, accepted for publication.

[17] T. Yamaguchi, *J. Phys. Chem. B*, 2018, 122, 1255–1260.

[18] J. P. Hansen and I. R. McDonald, *Theory of Simple Liquids*, 2nd edn., Academic Press, 1986.

[19] J. P. Boon and S. Yip, *Molecular Hydrodynamics*, McGraw-Hill, 1980.

[20] F. Hirata, *Theory of Molecular Liquids*, in *Molecular Theory of Solvation*, F. Hirata ed., Kluwer, 2003.

[21] T. Yamaguchi and S. Koda, *J. Chem. Phys.*, 2010, **132**, 114502.

[22] X. Zhong, Z. Liu and D. Cao, *J. Phys. Chem. B*, 2011, **115**, 10027-10040.

[23] M. J. Abraham, T. Murtola, R. Schulz, S. Pall, J. C. Smith, B. Hess, and E. Lindahl, *SoftwareX*, 2015, **1-2**, 19–25.

[24] B. Hess, H. Bekker, H. J. C. Berendsen, and J. G. E. M. Fraaije, *J. Comp. Chem.*, 1997, **18**, 1463–1472.

[25] H. Tokuda, H. Hayamizu, K. Ishii, M. A. B. H. Susan and M. Watanabe, *J. Phys. Chem. B*, 2005, **109**, 6103-6110.

[26] T. Yamaguchi, S. Miyake and S. Koda, *J. Phys. Chem. B*, 2010, **114**, 8126–8133.

[27] T. Yamaguchi, E. Nakahara, K. Sueda and S. Koda, *J. Phys. Chem. B*, 2013, **117**, 4121–4126.

[28] R. Böhmer, C. Gainaru and R. Richert, *Phys. Rep.*, 2014, **545**, 125–195.

[29] S. P. Bierwirth, J. Bolle, S. Bauer, C. Sternemann, C. Gainaru, M. Tolan and R. Böhmer, *Scaling of suprastructure and dynamics in pure and mixed Debye liquids*, in *The scaling of relaxation processes*, A. Loidl and F. Kremer ed., Springer, 2018.

[30] U. Kaatze and R. Behrends, *Int. J. Thermophys.*, 2014, **35**, 2088−2106.

[31] C. Gainaru, R. Figuli, T. Hecksher, B. Jakobsen, J. C. Dyre, M. Wilhelm and R. Böhmer, *Phys. Rev. Lett.*, 2014, **112**, 098301.

[32] C. Gainaru, M. Wikarek, S. Pawlus, M. Paluch, R. Figuli, M. Wilhelm, T. Hecksher, B. Jakobsen, J. C. Dyre and R. Böhmer, *Colloid Polym. Sci.*, 2014, **292**, 1913−1921.

[33] T. Yamaguchi, M. Saito, K. Yoshida, T. Yamaguchi, Y. Yoda and M. Seto, *J. Phys. Chem. Lett.*, 2018, **9**, 298–301 (2018).

[34] T. Yamaguchi, *J. Chem. Phys.*, 2017, **146**, 094511.